Slices of the Kerr ergosurface

Ted Jacobson and Yee-Ann Soong

Center for Fundamental Physics, Department of Physics, University of Maryland, College Park, MD 20742-4111, USA

E-mail: jacobson@umd.edu and soongy@umd.edu

Abstract
The intrinsic geometry of the Kerr ergosurface on constant Boyer–Lindquist (BL), Kerr and Doran time slices is characterized. Unlike the BL slice, which had been previously studied, the other slices (i) do not have conical singularities at the poles (except the Doran slice in the extremal limit), (ii) have finite polar circumference in the extremal limit and (iii) for sufficiently large spin parameter fail to be isometrically embeddable as a surface of revolution above some latitude. The Doran slice develops an embeddable polar cap for spin parameters greater than about 0.96.

PACS number: 04.70.Bw

(Some figures in this article are in colour only in the electronic version)

1. Introduction

The ergosurface of the Kerr spacetime is the locus at which the asymptotic time translation symmetry becomes lightlike. This symmetry is spacelike inside the ergosurface, so negative energy states of matter are allowed there [1]. The existence of these negative energy states is probably central to the mechanism by which rotational energy is extracted from astrophysical black holes [2, 3]. The Penrose process [1, 4] is an idealized example of such a mechanism, whose discovery led directly to the realization that black holes behave as thermodynamic systems in equilibrium, with an entropy proportional to the surface area of the event horizon and a temperature proportional to the surface gravity [5].

Given the importance of the ergosurface, it is natural to examine its intrinsic two-dimensional (2D) geometry. While this geometry plays no direct role in dynamical processes, it could be useful for physical intuition and visualization, and is in any case mathematically interesting. Unlike the event horizon, however, the ergosurface is not a null surface, and therefore different spacelike slices of it determine different 2D geometries. In this paper we examine and compare the geometry of three different slices, those defined by the Boyer–Lindquist (BL), Kerr and Doran [6] time coordinates.

The geometry of the BL slice has already been extensively studied [7–9]. Peculiar features of that geometry are that the poles have conical singularities, and that in the limit of maximal rotation (extreme Kerr geometry) the surface becomes infinitely long in the polar direction. This happens because the ergosurface coincides with the horizon at the poles, and the horizon recedes to infinite distance on a surface of constant BL time coordinate in the extremal limit. By contrast, the horizon remains at a finite separation on constant Kerr or Doran time surfaces, since these surfaces are defined by geodesics freely falling across the horizon.

The remainder of this paper is organized as follows. In section 2 we present the Kerr metric in the three different coordinate systems and obtain the 2D metrics for the corresponding ergosurface slices. Section 3 discusses general properties of axisymmetric 2D geometries, and section 4 presents the results for the slices of the Kerr ergosurface. Mathematica was used for most of the computations.

2. Kerr spacetime and the ergosurface

The Kerr black hole spacetime has both time translation symmetry and axial rotation symmetry. The BL, Kerr and Doran coordinate systems all have in common two coordinates, called r and θ, which are constant in these symmetry directions. The remaining two coordinates are (t, ϕ) for BL, $(\tilde{t}, \tilde{\phi})$ for Kerr ($\tilde{t}$ is commonly called v) and $(\bar{t}, \bar{\phi})$ for Doran. The 'time' coordinates $t, \tilde{t}$ and $\bar{t}$ differ from each other only by the addition of a function of r, as do the azimuthal angle coordinates $\phi, \tilde{\phi}$ and $\bar{\phi}$. The relation between the time coordinates is given by

$$\mathrm{d}t + \frac{\beta}{1 - \beta^2}\,\mathrm{d}r = \mathrm{d}\bar{t} = \mathrm{d}\tilde{t} - \frac{1}{1 + \beta}\,\mathrm{d}r \tag{1}$$

and the angles are related by

$$\mathrm{d}\phi + \frac{\beta}{1 - \beta^2}\frac{a}{r^2 + a^2}\,\mathrm{d}r = \mathrm{d}\bar{\phi} = \mathrm{d}\tilde{\phi} - \frac{1}{1 + \beta}\frac{a}{r^2 + a^2}\,\mathrm{d}r \tag{2}$$

with

$$\beta^2 = 2Mr/(r^2 + a^2), \tag{3}$$

where M and a are the mass and spin parameter (angular momentum divided by mass) of the Kerr spacetime, and β is the positive root of (3).

The line element in these three coordinate systems takes the form

$$\begin{aligned}\mathrm{d}s^2 &= -(1 - \alpha^2)\,\mathrm{d}t^2 + \alpha^{-2}\beta^2(1 - \beta^2)^{-1}\,\mathrm{d}r^2 - 2\alpha^2 a \sin^2\theta\,\mathrm{d}t\,\mathrm{d}\phi \\ &\quad + \rho^2\,\mathrm{d}\theta^2 + (r^2 + a^2 + \alpha^2 a^2 \sin^2\theta)\sin^2\theta\,\mathrm{d}\phi^2\end{aligned} \tag{4}$$

$$\begin{aligned}&= -(1 - \alpha^2)\,\mathrm{d}\tilde{t}^2 + 2(\mathrm{d}\tilde{t} - a \sin^2\theta\,\mathrm{d}\tilde{\phi})\,\mathrm{d}r - 2\alpha^2 a \sin^2\theta\,\mathrm{d}\tilde{t}\,\mathrm{d}\tilde{\phi} \\ &\quad + \rho^2\,\mathrm{d}\theta^2 + (r^2 + a^2 + \alpha^2 a^2 \sin^2\theta)\sin^2\theta\,\mathrm{d}\tilde{\phi}^2\end{aligned} \tag{5}$$

$$\begin{aligned}&= -\mathrm{d}\bar{t}^2 + (\alpha^{-1}\beta\,\mathrm{d}r + \alpha(\mathrm{d}\bar{t} - a \sin^2\theta\,\mathrm{d}\bar{\phi}))^2 \\ &\quad + \rho^2\,\mathrm{d}\theta^2 + (r^2 + a^2)\sin^2\theta\,\mathrm{d}\bar{\phi}^2,\end{aligned} \tag{6}$$

where

$$\alpha^2 = 2Mr/\rho^2 \qquad \text{and} \qquad \rho^2 = r^2 + a^2 \cos^2\theta, \tag{7}$$

and α is the positive root. Note that, since the coordinates differ only by functions of r, the coefficients of all terms not involving $\mathrm{d}r$ are equal for the three coordinate systems.

We now summarize some key properties of the Kerr geometry in these coordinates. In BL coordinates the metric has just one off-diagonal ($dt\,d\phi$) term, and the constant t surfaces are orthogonal to stationary, zero angular momentum observers (ZAMO's). In Kerr coordinates (which are sometimes called advanced Eddington–Finkelstein coordinates by analogy with the non-rotating, Schwarzschild case) the curves $d\theta = d\tilde{\phi} = d\tilde{t} = 0$ are lightlike geodesics with zero angular momentum and affine parameter r. The surfaces of constant $\tilde{t}$ are *timelike*, so $\tilde{t}$ is actually a 'space coordinate' rather than a time coordinate. (In the non-rotating case it is lightlike.) In Doran coordinates, the curves $d\theta = d\bar{\phi} = \beta dr + \alpha^2 d\bar{t} = 0$ are timelike geodesics with zero angular momentum, unit energy (at rest at infinity) and proper time $\bar{t}$. The surfaces of constant $\bar{t}$ are orthogonal to these geodesics.

The event horizon of the black hole is located where $\beta = 1$, i.e.

$$r_h = M + (M^2 - a^2)^{1/2}. \tag{8}$$

The BL t coordinate is singular at the horizon, where it runs to infinity. This can be seen in the coordinate transformation (1). The relation between $\bar{t}$ and $\tilde{t}$ on the other hand is finite in this limit. Similar relations hold between the various angle coordinates.

The ergosurface occurs where the time translation symmetry becomes lightlike, at $\alpha = 1$, i.e.

$$r_e(\theta) = M + (M^2 - a^2 \cos^2 \theta)^{1/2}. \tag{9}$$

This surface coincides with the horizon at the poles, but lies outside the horizon at all other latitudes. On this surface dr is related to $d\theta$ via

$$dr = \frac{dr_e}{d\theta} d\theta = \frac{a^2 \cos\theta \sin\theta}{(M^2 - a^2 \cos^2\theta)^{1/2}} d\theta. \tag{10}$$

We are interested in the 2D intersection of the ergosurface with a surface of constant t, $\tilde{t}$, or $\bar{t}$. The line element restricted to these 2D surfaces is as follows:

(BL) $2r_e\, d\theta^2 + 2(r_e + a^2 \sin^2\theta) \sin^2\theta\, d\phi^2 + \beta^2(1 - \beta^2)^{-1}\, dr^2$ \hfill (11)

(Kerr) $2r_e\, d\theta^2 + 2(r_e + a^2 \sin^2\theta) \sin^2\theta\, d\tilde{\phi}^2 - 2a \sin^2\theta\, dr\, d\tilde{\phi}$ \hfill (12)

(Doran) $2r_e\, d\theta^2 + 2(r_e + a^2 \sin^2\theta) \sin^2\theta\, d\bar{\phi}^2 + \beta^2\, dr^2 - 2\beta a \sin^2\theta\, dr\, d\bar{\phi}$, \hfill (13)

where dr is given by (10), and we have adopted units with $M = 1$. In the limiting case $a = 0$, the ergosurface coincides with the horizon, which sits at fixed radius. All three slices then coincide, and the geometry is just a 2-sphere of radius $r_h = 2M$.

3. Axisymmetric 2D geometry

The three 2D metrics (11)–(13) all take the form

$$A\, d\theta^2 + 2B\, d\theta\, d\phi + R^2\, d\phi^2, \tag{14}$$

where A, B and R are functions only of θ, and are symmetric under reflection about the equator $\theta = \pi/2$. R is the circumferential radius of the symmetry circles, i.e. the lines of latitude (constant θ), and is the same in all three cases,

$$R = (2r_e(\theta) + 2a^2 \sin^2\theta)^{1/2} \sin\theta. \tag{15}$$

Changing coordinates via

$$d\hat{\phi} = d\phi + (B/R^2)\, d\theta, \qquad du = (A - B^2/R^2)^{1/2}\, d\theta \tag{16}$$

3

puts (14) into the standard form

$$du^2 + R^2 \, d\hat{\phi}^2. \tag{17}$$

The intrinsic geometry is fully described by the function $R(\theta(u))$, which gives the circumferential radius as a function of perpendicular distance u from the pole. The range of u (unlike θ) represents a geometrically intrinsic property, and is given by the integral of du over θ from 0 to π.

The Gaussian curvature k of the surface provides a purely local handle on the geometry. For the metric (17) it is given by

$$k = -R_{,uu}/R \tag{18}$$

where the comma denotes derivative with respect to the following variable. This may be expressed in terms of derivatives with respect to θ using the chain rule, which yields

$$k = -\frac{R_{,\theta\theta}}{R(A - B^2/R^2)} + \frac{R_{,\theta}(A - B^2/R^2)_{,\theta}}{2R(A - B^2/R^2)^2}. \tag{19}$$

Note that since the radius R goes to zero at the poles, the curvature (18) diverges there unless $R_{,uu}$ approaches zero at least as fast as R.

Even if the curvature remains finite as the pole is approached, there is a conical singularity at $\theta = 0$ unless $R_{,u} \to 1$. Indeed, if $R = \sigma u + O(u^2)$, one can absorb the constant factor σ into a rescaled angle $\sigma\hat{\phi}$, which then ranges from 0 to $2\pi\sigma$. The deficit angle is thus given by $\delta = 2\pi(1 - \sigma)$, where $\sigma = R_{,u}(u = 0)$. In terms of the original metric coefficients, this may be expressed as

$$\delta = 2\pi \left(1 - \frac{R_{,\theta}}{(A - B^2/R^2)^{1/2}}\right)_{\theta \to 0}. \tag{20}$$

In the BL case $B = 0$, and in the other two cases B vanishes fast enough with θ that it does not contribute to (20), hence for the cases at hand we have the simpler formula

$$\delta = 2\pi(1 - R_{,\theta}/A^{1/2})_{\theta \to 0}. \tag{21}$$

The surface is isometrically embeddable as a surface of revolution (hereafter just 'embeddable') in 3D Euclidean space with cylindrical coordinates $(R, \hat{\phi}, z)$ if and only if there exists a real height function $z(R)$ such that

$$du^2 = dR^2 + d(z(R))^2, \tag{22}$$

where $d(z(R)) = z_{,R} \, dR$. Such a function exists if and only if $dR \leqslant du$, i.e. $R_{,u} \leqslant 1$.[1] That is, if the surface is to be embeddable then R must not grow faster than u.[2] When it exists, $z(R(u))$ is determined by the differential equation

$$dz/du = (1 - (R_{,u})^2)^{1/2}. \tag{23}$$

In terms of the original coordinate θ and the original metric functions this becomes[3]

$$\frac{dz}{d\theta} = (A - B^2/R^2 - (R_{,\theta})^2)^{1/2}. \tag{24}$$

Note that the embeddability condition $R_{,u} \leqslant 1$ is independent of the sign of the curvature (18), i.e. the sign of $-R_{,uu}$.

---

[1] If $R_{,u} > 1$ then (22) implies $dz^2 < 0$, so dz is pure imaginary. One can then identify $|dz|$ as the change of a time coordinate in a 3D Minkowski space, thus determining a Minkowskian embedding, as was done in [7].

[2] If the condition that the embedding be a surface of revolution is dropped then, according to the Janet–Cartan theorem, any analytic 2D metric can be locally isometrically embedded in 3D Euclidean space [10].

[3] Sharp [7] states that no axisymmetric embedding exists if $B \neq 0$. This is evidently untrue as long as one allows for a θ-dependent shift (16) of $\hat{\phi}$ relative to ϕ.
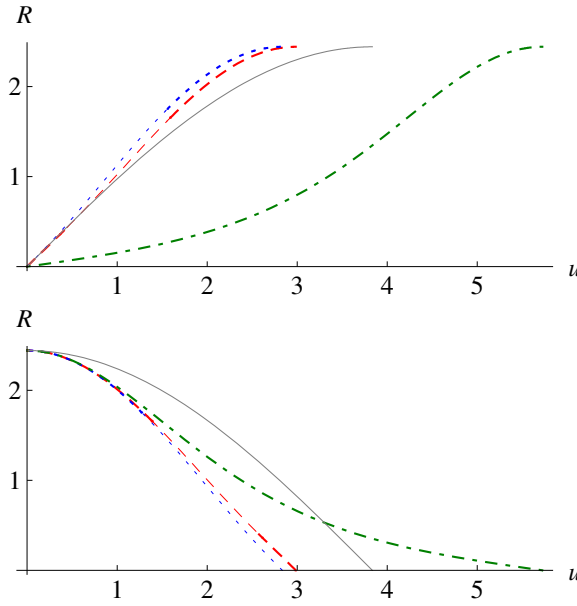
Figure 1. Circumferential radius R of latitude circles versus longitudinal distance u for $a = 0.99$. In the upper graph the range of u runs from 0 at the pole to its value at the equator (which is different for each slice). In the lower graph u runs in the opposite direction, with $u = 0$ at the equator rather than at the pole. The BL curve is dot-dashed green, the Kerr curve is dotted blue and the Doran curve is dashed red. For comparison, the solid gray line displays the graph for a round sphere with the same equatorial circumference. The curves (other than that for the sphere) are thick where the surface is embeddable (i.e., where the magnitude of the slope is less than unity), and thin where it is not. The sign of the Gaussian curvature k at each u is opposite to the curvature of the graph, according to (18).

4. Geometries of Kerr ergosurface slices

As stated above, in the non-rotating limit the BL, Kerr and Doran slices of the ergosurface all coincide with a 2-sphere of radius $2M$. As a grows, the slices deviate increasingly from each other, becoming maximally different in the extremal case $a = M$. (We do not consider trans-extremal cases here.) The Kerr and Doran $R(u)$ functions are extremely close to each other until a is very close to unity, e.g. for $a = 0.7\,M$ they differ by less than 1%, while the BL slice deviates significantly for smaller values of a. In the remainder of this section we adopt units with $M = 1$.

A representative example is shown in figure 1 which displays numerically generated plots of R (circumference/2π) versus u (longitudinal distance) for the highly spinning case $a = 0.99$. The content of these two figures is the same, except the different cases are aligned at the pole in the upper figure and at the equator in the lower figure, to better compare the geometries. The legend scheme is explained in the figure caption, and is maintained for all the following plots.

The BL slice (dot-dashed green) curvature is positive below some latitude and negative above. The distance from equator to pole is much longer than for the other slices, and in fact grows without bound as a approaches unity. There is a conical deficit at the pole, indicated by the slope of $R(u)$ which is less than unity at $u = 0$. In fact there is a conical singularity on
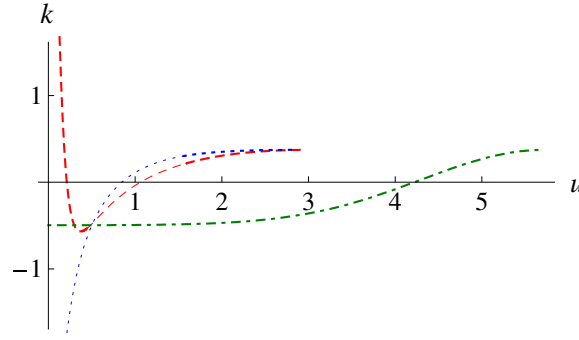
5

Figure 2. Curvature versus polar distance, $a = 0.99$. The curvature is positive at the equator, and becomes negative at a higher latitude. On the Doran slice it turns around and goes to positive values near the pole. As in the previous figures, the curves are thick where the surface is embeddable. Note that the sign of the curvature does not determine embeddability.

the BL slice for all nonzero values of a, with deficit angle (21) given by $2\pi(1 - (1 - a^2)^{1/2})$. The BL slice is globally embeddable for all values of a. (These results for the BL case were previously obtained in [7–9].)

The Kerr slice (dotted blue) curvature is also positive below some latitude and negative above. The distance from equator to pole remains finite as a approaches unity. The slope of $R(u)$ at $u = 0$ is unity so the geometry is smooth at the pole, i.e. there is no conical deficit, as can easily be verified directly using (21) for all values of a. The curvature is negative at the pole, where the slope is increasing from unity ($R_{,uu} > 0$). When the slope begins decreasing the curvature becomes positive, but the surface remains non-embeddable until the slope drops down below unity, which for the example shown occurs around $u \approx 1.5$.

The Doran slice (dashed red) curvature is positive at the equator, becomes negative above some latitude, and then becomes positive again near the pole. Like for the Kerr slice, the distance to the pole remains finite for $a = 1$, and the geometry is smooth at the pole (except for $a = 1$, as discussed below). The example shown in figure 1 is embeddable in a polar cap region $u \lesssim 0.4$ as well as for an equatorial region $u \gtrsim 1.5$. (An embeddable polar region occurs for a greater than a value between 0.95 and 0.96.) Moving from the equator to the pole, the curvature turns negative roughly halfway through the non-embeddable region and becomes positive again roughly halfway through the embeddable polar cap.

4.1. Curvature

The curvature at the equator is the same on all three slices, and equal to $k_{eq} = (4 + 5a^2)/(16 + 8a^2)$. The non-spinning case has $k_{eq} = 1/4$ and the extremal case has $k_{eq} = 3/8$. To see why it is the same on all the slices, note that the geometry is reflection symmetric about the equatorial plane, so dr vanishes there; in fact, as (10) shows, it vanishes as $\cos\theta$. Thus the metric components on the equator agree for all three slices. Moreover, reflection symmetry implies $R_{,\theta} = 0$, so the second term of (19) vanishes, and the first term of (19) agrees since A and B agree on the equator and R agrees everywhere.

The curvature as a function of polar distance is shown in figure 2 for the representative case $a = 0.99$. For all three slices the curvature is positive at the equator, and becomes negative at a higher latitude. It levels out as the pole is approached on the BL slice, keeps dipping to lower values on the Kerr slice, and on the Doran slice it turns around and goes to positive values near the pole.
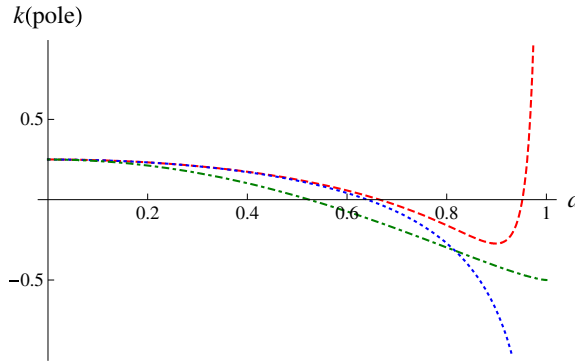
6

k(pole)

Figure 3. Curvature at the pole versus spin parameter a. All three slices have positive curvature at the pole for sufficiently small values of a, and they first develop negative curvature for a approximately equal to $0.52, 0.64$ and 0.67 in the BL, Kerr and Doran cases, respectively. They have rather different behavior as a grows close to 1. The polar curvature goes to $-1/2$ in the BL case, and diverges negatively in the Kerr case. In the Doran case it becomes positive again for a greater than approximately 0.95, and diverges positively as a approaches 1. A polar region is embeddable in the Kerr and Doran cases if and only if the curvature at the pole is positive.

The curvature at the pole itself is shown as a function of a in figure 3. In the BL case this is the limiting curvature as the conical singularity at the pole is approached. In the Kerr and Doran cases, the geometry at the pole is smooth so, as explained in section 3, $R_{,u} = 1$ there. Thus for positive curvature ($-R_{,uu} > 0$) at the pole, a polar region with $R_{,u} < 1$ exists, which is embeddable, while for negative curvature it is not embeddable at the pole.

In the precisely extremal case $a = 1$, the curvature approaching the pole diverges negatively as $-u^{-1}$ on both the Kerr and Doran slices. This appears at first to contradict figures 2 and 3 which show a *positive* divergence of the curvature in the Doran case. The resolution of this apparent contradiction is that, as $a \to 1$, the polar region of positive curvature contracts to an infinitesimal region including only the pole itself. The asymptotic behavior $-u^{-1}$ describes an infinite negative dip before this infinitely narrow, infinitely positive spike.

4.2. Embedding diagrams

An embedding diagram for the region including the equator is shown in figure 4 for the case $a = 0.99$. An embedding diagram for the Doran polar cap is shown separately in figure 5, for a sequence of increasing values of a. As a approaches closer to unity, the embedding is more sharply curved at the pole. In the limiting case $a = 1$ it develops a conical singularity at the pole. The reason is that, rather than vanishing at the pole, dr is given by $a\, d\theta$, since the denominator of (10) vanishes as $\sin\theta$, canceling the $\sin\theta$ in the numerator. The deficit angle, calculated from (21), is found to be $2\pi(1 - \sqrt{2/3})$.

The polar cap could be placed in a common embedding diagram with the equatorial region, faithfully showing the R values relative to a common axis. However, the relative position in the z direction would have no significance since these two patches are not joined by an embedding. Also, the sign of z has no effect on the induced geometry of the embedded surface, so the polar cap embedding could just as well be displayed reflected across the R-axis, as a bump rather than as a dimple at the pole. We have chosen to display it as a dimple in figure 5 just because, if the radial distance in the embedding space is (incorrectly) identified with this r coordinate, the increase of the r coordinate of the ergosurface (9) with θ is mimicked.
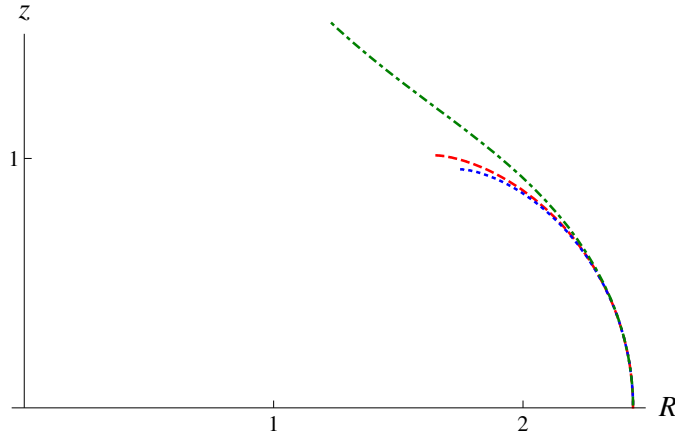
Figure 4. Embedding of equatorial region, $a = 0.99$. The surface of revolution is generated by reflecting the graph across the R-axis and then rotating about the z-axis. The curve for the BL slice is truncated at $z = 1.5$. When continued, it tapers to a conical singularity at the axis. The Kerr and Doran slice embeddings are rather similar to each other. As implied by (23), the slope dz/dR vanishes at the point where the embedding fails to exist.
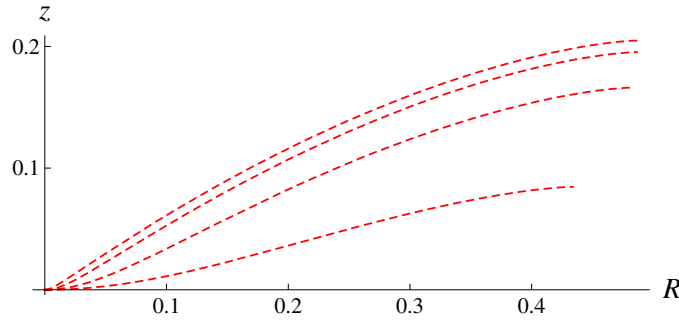

Figure 5. Embedding of Doran polar region, $a = 0.99, 0.999, 0.9999, 0.99999$. In the limiting case $a = 1$ a conical singularity develops at the pole.

5. Summary

We have analyzed and compared the geometries of three different spatial slices of the ergosurface of the Kerr spacetime, corresponding to constant values of Boyer–Lindquist, Kerr and Doran time coordinates. We found that, unlike the BL slice which has a conical singularity, both the Kerr and Doran slices are smooth at the pole, except for the extremal case of the Doran slice. Also unlike the BL slice, the distance from equator to pole remains finite as the spin parameter a approaches the extremal value M. All the slices develop negative curvature above some latitude for sufficiently high spin, and the Doran slice develops also a positive curvature polar cap above $a \approx 0.95\,M$. In the extremal limit $a = M$ this becomes a conical singularity at the pole, with a deficit angle $2\pi(1 - \sqrt{2/3})$.

The slices differ in where they can be isometrically embedded as surfaces of revolution in a 3D Euclidean space. The BL slice is fully embeddable for all spin parameters, and the

Kerr and Doran slices fail to be embeddable above some latitude when the spin parameter is sufficiently large. For spin parameter $a \gtrsim 0.96\,M$ the Doran slice is also embeddable at high latitudes, in a polar cap. We showed some embedding diagrams, and indicated the embeddable regions on plots of circumference versus radius. These plots allow easy comparison of the geometries of the three slices.

Acknowledgment

References

[1] Penrose R 1969 Gravitational collapse: the role of general relativity *Riv. Nuovo Cimento* **1** 252
    Penrose R 2002 Gravitational collapse: the role of general relativity *Gen. Rel. Grav.* **34** 1141
[2] Begelman M C, Blandford R D and Rees M J 1984 Theory of extragalactic radio sources *Rev. Mod. Phys.* **56** 255
[3] Meier D L, Koide S and Uchida Y 2001 Magnetohydrodynamic production of relativistic jets *Science* **291** 84
[4] Penrose R and Floyd R M 1971 Extraction of rotational energy from a black hole *Nature* **229** 177
[5] Bekenstein J D 1973 Black holes and entropy *Phys. Rev.* D **7** 2333
[6] Doran C 2000 A new form of the Kerr solution *Phys. Rev.* D **61** 067503 (arXiv:gr-qc/9910099)
[7] Sharp N A 1981 On embeddings of the Kerr geometry *Can. J. Phys.* **59** 688
[8] Kokkotas K D 1988 The geometry of the Kerr–Newman ergosurface *Gen. Rel. Grav.* **20** 829
[9] Pelavas N, Neary N and Lake K 2001 Properties of the instantaneous ergo surface of a Kerr black hole *Class. Quantum Grav.* **18** 1319 (arXiv:gr-qc/0012052)
[10] Han Q and Hong J-X 2006 *Isometric Embedding of Riemannian Manifolds in Euclidean Spaces (Mathematical Surveys and Monographs* vol 130*)* (Providence, RI: American Mathematical Society)